J. Phys. B: At. Mol. Opt. Phys. 26 (1993) 3937–3949. Printed in the UK

# Hyperspherical approach to Coulombic three-body systems with different masses

Yan Zhou†, C D Lin† and J Shertzer

† Department of Physics, Kansas State University, Manhattan, KS 66506, USA
‡ College of the Holy Cross, Worcester, MA 01610, USA

Received 10 May 1993, in final form 12 July 1993

**Abstract.** We adopted mass-weighted hyperspherical coordinates to study the properties of Coulombic three-body systems where all three particles are different. Using an adiabatic approximation, we applied the finite-element method to the two-dimensional eigenvalue problems at fixed hyperradius. We have calculated the adiabatic hyperspherical potential curves, and examined the wavefunctions (in terms of density plots) and the non-adiabatic coupling terms for a number of three-body systems. By fixing the masses of two of the particles, we examined how these properties vary with the mass of the third particle. The existence of stable bound states versus the masses of the systems is also investigated.

## 1. Introduction

The non-relativistic three-body systems consisting of three charged particles have been studied extensively over the years. In general, it is important to distinguish systems where two of the three particles are identical (to be called AAB systems hereafter) from systems where all three are different (to be called ABC systems). The indistinguishability of the two identical particles poses constraints on the symmetry of the wavefunctions. It has been proved that in all Coulombic AAB systems there exists at least one stable bound state (Hill 1977). Using the exponential trial functions in the relative coordinates the ground state energies of the AAB systems have been calculated accurately (Frolov 1987). Furthermore, it has been observed that the total binding energy of an AAB system nearly scales with the reduced mass of A and B (Chen and Lin 1990). For the higher excited states it has been further shown that many properties of the AAB systems depend weakly on the relative masses of A and B (Liu *et al* 1991). This weak mass dependence also reflects in that doubly excited states of atomic systems such as $H^-$ and He exhibit ro-vibrational energy level structure similar to those in molecules (Herrick *et al* 1980, Lin 1984, 1986). It further suggests why the molecular interpretation is reasonably successful in qualitatively explaining the structure and dynamics of doubly excited states of atoms (Rost and Briggs 1991, Berry and Krause 1988).

In the last few years a unifying approach for treating non-relativistic three-body systems in mass-weighted hyperspherical coordinates has been proposed (Lin and Liu 1988). The method has been applied to examine properties of excited states of an AAB system as a function of the mass ratio $\lambda = m_A/m_B$ (Liu *et al* 1991). It was shown that for a fixed angular momentum and parity of the system, the adiabatic hyperspherical potential curves are very insensitive to the mass ratio $\lambda$ and that the shape of the corresponding states, as exhibited by the density distribution of the wavefunctions, is also very similar.

0953-4075/93/213937+13$07.50  

In this paper, we study the properties of Coulombic three-body systems where all three particles are different using mass-weighted hyperspherical coordinates. We will consider systems where the charge on each particle is one unit, and the signs of the charges of A and B are identical and $m_A \geqslant m_B$ . Atomic units are used unless otherwise noted. Furthermore we set $m_C = 1$. Obviously we can use $A^+B^+C^-$ to represent such three-body systems. Note that two-body bound states can be formed for either of the $A^+C^-$ or the $B^+C^-$ pairs.

For the ABC systems, there is only a certain range of $m_A$ and $m_B$ (with $m_C = 1$) where the system can have stable ground states. The range of masses for such stability to exist has been investigated by a number of authors using variational methods (Poshusta 1985, Gur'yanov and Rebane 1991, Frolov and Thakkar 1992, Bishop and Frolov 1992, Martin *et al* 1992). We will examine a number of systems by calculating the hyperspherical potential curves which will give indications of the existence of bound states. Our major goal, however, is to study scattering states as well. In particular, our final goal is to develop a computational procedure based on the hyperspherical coordinates method for calculating inelastic excitation and rearrangement collision cross sections. Such an approach based on the hyperspherical method has been fully developed for two-electron systems where the mass of the nucleus is much heavier than that of the electron and thus the centre of mass can be considered to be stationary (Tang *et al* 1992). To apply the hyperspherical approach to general three-body systems, a number of numerical methods have to be developed. The basic nature of the three-body systems, in terms of adiabatic potential curves and adiabatic wavefunctions, should be examined before scattering calculations are actually carried out. In this paper we study the three-body systems within the adiabatic approximation, to examine the potential curves, the wavefunctions and the coupling terms, so as to follow how these quantities vary with the masses of the system.

The present mass-weighted hyperspherical approach has been used by quantum chemists for calculating reactive scattering cross sections (Launay and Le Dourneuf 1989, 1990, Pack and Parker 1989). It has been applied by Archer *et al* (1990) in calculating the positronium formation cross sections. When applying the method to Coulomb problems, the singularity of Coulomb potentials poses numerical difficulties not encountered in chemical reactive scatterings. Furthermore, the higher precision in atomic physics requires that all the numerical calculations be carried out to at least five digits accuracy. This was not possible in most of the numerical codes that have been used. For example, Archer *et al* (1990) stated that they can only achieve two digits accuracy in the potential curves at large distances.

After a brief review of the basic formulation in section 2, we present the higher-order finite element method used in our numerical calculations in section 3. The results are presented in section 4, together with a discussion of the general trends. The paper finishes with a brief summary and discussions of future developments. We should mention that the present hyperspherical approach has been used by a number of authors in a more limited sense and that the numerical approaches are rather different, see Hara *et al* (1988), Hara and Ishihara (1989), Fukuda *et al* (1990) and Botero and Greene (1985).

## 2. Summary of the hyperspherical methodology and the potential surfaces

### *2.1. The coordinate systems*

We briefly summarize the coordinate systems and the notations used in this article. The three particles are denoted by A, B and C, respectively, each carries one unit of charge, and can be designated as $A^+B^+C^-$ in general. Since charge conjugation applies, there is no

difference between this system and the $A^-B^-C^+$ system. We also choose the convention that $m_A \geqslant m_B$. In the dissociation limit, particles B and C can form 'hydrogenic' bound states, with energies given by $-\mu_{BC}/2n^2$ in atomic units, where $\mu_{BC}$ is the reduced mass of B and C and $n$ is the principal quantum number. Similar bound states can be formed by particles A and C. For the same $n$, the binding energy of the AC system is larger than that of the BC system because of the larger reduced mass $\mu_{AC}$.

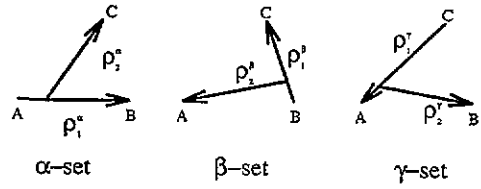


**Figure 1.** Definitions of the three sets of Jacobi coordinates. The convention is that the charges of particles A and B have the same sign, and charge of particle C has the opposite sign to that of A or B. The convention $m_A \geqslant m_B$ is adopted.

For a given ABC system, we can choose three sets of Jacobi coordinates, see figure 1. Note that the $\beta$-set is convenient for describing the scattering states for A + (BC), where (BC) is a two-body bound state, and the $\gamma$-set is convenient for describing the scattering of B + (AC). The advantage of the $\alpha$-set is less obvious, but it is important to recognize that in the $\alpha$-set, the line joining A and B is a symmetry axis if A and B are two identical particles. Furthermore, if both A and B are much heavier than C, the line joining A and B is a 'molecular' axis which is approximately a good quantization axis according to the Born–Oppenheimer approximation.

Starting with each set of Jacobi coordinates, we can define two mass-weighted vectors $\xi_1$ and $\xi_2$ (Liu *et al* 1991)

$$\xi_1 = \sqrt{(\mu_1/\mu)}\rho_1 \qquad \xi_2 = \sqrt{(\mu_2/\mu)}\rho_2. \tag{1}$$

where $\rho_1$ and $\rho_2$ are defined in figure 1 and $\mu_1$ and $\mu_2$ are the reduced masses associated with the 'pair' of particles connected by each vector, respectively, and $\mu$ is arbitrary. For each set of coordinates we can define a hyperradius $R$ and a hyperangle $\phi$:

$$R^2 = \xi_1^2 + \xi_2^2 \qquad \tan\phi = \xi_2/\xi_1 \tag{2}$$

where $R$ is invariant among the three set of coordinates, but $\phi$ depends on the specific Jacobi coordinates. For convenience, we also define a 'regular' hyperspherical angle $\chi$:

$$\tan\chi = \rho_2/\rho_1 = \sqrt{(\mu_2/\mu_1)}\tan\phi. \tag{3}$$

Thus $\chi$ is a measure of the 'actual' distances $\rho_1$ and $\rho_2$ . The $\chi$ angle also depends on the Jacobi coordinate system used.

It should be pointed out that there are various ways of defining the five angles in the hyperspherical approach, even though the definition of the mass-weighted hyperradius is the same. A complete list of references on hyperspherical coordinates up to 1989 can be found in the monograph by Avery (1989). Our present choice is convenient for transforming the wavefunctions in hyperspherical coordinates to those given in the independent particle coordinates in the asymptotic region. This latter procedure is anticipated when the present method is extended to scattering problems.

### 2.2. *The potential surfaces*

Using the mass-weighted hyperspherical coordinates, the kinetic energy operators for all the three-body systems are identical, and the mass dependence enters only through scaling factors in the potential. Using the $\alpha$-set coordinates, the potential surface is

$$V(R,\phi,\theta) = C(\phi,\theta)/R \tag{4}$$

where $\theta$ is the angle between the two vectors $\xi_1$ and $\xi_2$ and

$$C = \frac{Z_A Z_B}{\cos\phi^\alpha}\left(\frac{\mu_1^\alpha}{\mu}\right)^{1/2} + \frac{Z_B Z_C}{\cos\phi^\beta}\left(\frac{\mu_1^\beta}{\mu}\right)^{1/2} + \frac{Z_C Z_A}{\cos\phi^\gamma}\left(\frac{\mu_1^\gamma}{\mu}\right)^{1/2}. \tag{5}$$

The potential surface has two valleys, with singularities located at $(\phi^\alpha,\theta^\alpha) = (\phi_1,\pi)$ and $(\phi_2,0)$, where

$$\tan\phi_1 = [m_B m_C/m_A(m_A+m_B+m_C)]^{1/2} \tag{6}$$

and

$$\tan\phi_2 = [m_A m_C/m_B(m_A+m_B+m_C)]^{1/2}. \tag{7}$$

**Table 1.** The singularities of the potential surface for different masses of the Coulombic three-body systems as viewed in the $\alpha$-set coordinates. The singularities of the potential valleys are located at $(\phi^\alpha,\theta^\alpha) = (\phi_1,\pi)$ and $(\phi_2,0)$. In the table, $m_C = 1$. The angles $\chi^\alpha$ for the singularities are also shown.

| System (ABC) | $m_A$ | $m_B$ | $\phi_1$ | $\phi_2$ | $\chi_1$ | $\chi_2$ |
|---|---|---|---|---|---|---|
| tt$\mu$ | 26.58 | 26.58 | 7.74° | 7.74° | 26.57° | 26.57° |
| dt$\mu$ | 26.58 | 17.75 | 6.80° | 10.71° | 21.14° | 31.52° |
| pt$\mu$ | 26.58 | 8.88 | 5.47° | 15.99° | 14.06° | 36.86° |
| xt$\mu$ | 26.58 | 3.00 | 3.48° | 28.29° | 5.79° | 41.94° |
| t$\mu^+\mu^-$ | 26.58 | 1.00 | 2.08° | 43.96° | 2.08° | 43.94° |

For tt$\mu$, $\phi_1 = \phi_2 = 7.74°$. As $m_B$ decreases, $\phi_1$ decreases to a smaller angle, while $\phi_2$ increases to a larger angle. One can also use $\chi$ to express the angles at the valleys. In table 1, the locations of the potential valleys, $\chi_1$ and $\chi_2$, are listed for a number of systems.

Contour plots of the potential surfaces for a number of ABC systems are shown in figure 2 to illustrate the evolution of the positions of the potential surfaces on the $(\chi^\alpha,\theta^\alpha)$ plane as the mass of particle B is reduced, while the masses of A and C are fixed. Clearly, as $m_B$ becomes smaller and smaller compared to $m_A$, the $\chi$ angle for the potential valley on the $\theta^\alpha = \pi$ axis becomes smaller, while that for the potential valley on the $\theta^\alpha = 0$ axis becomes larger. Recall that the kinetic energy operators are identical for all the four systems shown, thus the origin of the difference in the properties of the three-body systems versus the masses will be attributed to the differences in these potential surfaces, as will be further discussed in section 3.

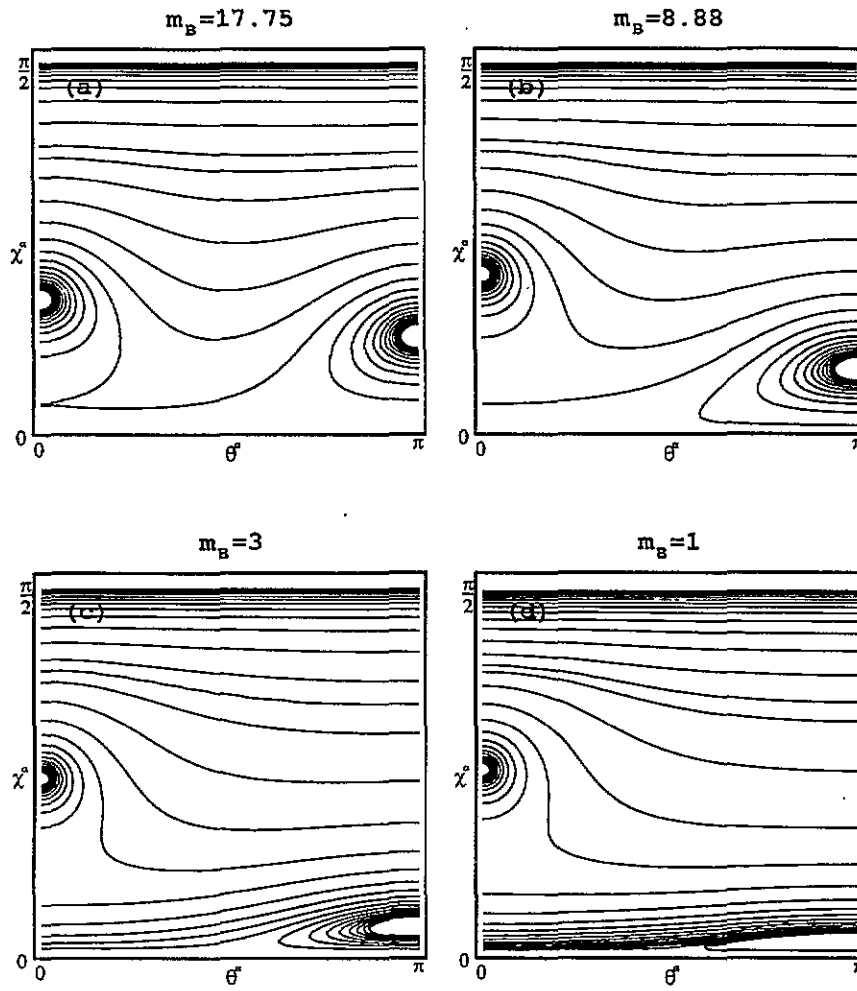


**Figure 2.** Contour plots of the potential surface for systems where $m_A = 26.58$, $m_C = 1$, and four different $m_B$ as shown in the $\alpha$-set hyperspherical coordinates. The singularities of the potential valleys at the $\chi$ angles are listed in table 1. (To illustrate the potential valleys more clearly, we actually plot the potential to the 2/3 power.)

### *2.3. The adiabatic approximation*

In this paper we will consider systems where the total angular momentum is zero. Since we do not include spin interactions, thus the total orbital angular momentum is zero and only three coordinates are needed to describe each system. We choose these three coordinates to be $R$, $\phi$ and $\theta$, where $\theta$ is the angle between the two vectors $\boldsymbol{\xi}_1$ and $\boldsymbol{\xi}_2$ and $\phi$ is defined in (2). We can use either of the three sets of Jacobi coordinates for defining $\phi$ and $\theta$, but the hyperradius is independent of these coordinate sets.

The Schrödinger equation in hyperspherical coordinates is

$$\left[-\frac{1}{2\mu}\left(\frac{\partial^2}{\partial R^2}+\frac{5}{R}\frac{\partial}{\partial R}-\frac{\Lambda^2(\phi,\theta)}{R^2}\right)+\frac{C(\phi,\theta)}{R}\right]\Psi(R,\phi,\theta)=E\Psi(R,\phi,\theta) \tag{8}$$

where the explicit expression for the grand angular momentum operator $\Lambda^2$ can be found

in Liu *et al* (1991). We expand (we use $\mu = (m_A + m_C)/m_A m_C$)

$$\Psi = (R^{5/2}\sin\phi\cos\phi)^{-1}\sum_{\mu} F_\mu(R)\Phi_\mu(R;\phi,\theta) \tag{9}$$

where $R$ is treated as an adiabatic parameter, and $\Phi_\mu(R;\phi,\theta)$ is the solution of the differential equation

$$\left[-\frac{\partial^2}{\partial\phi^2} - \frac{1}{\sin^2\phi\cos^2\phi\sin\theta}\frac{\partial}{\partial\theta}(\sin\theta\frac{\partial}{\partial\theta}) + 2\mu RC(\phi,\theta)\right]\Phi_\mu = R^2 U_\mu(R)\Phi_\mu \tag{10}$$

where $U_\mu(R)$ is the hyperspherical potential curve and $\Phi_\mu(R;\phi,\theta)$ is the channel function. The hyperradial function $F_\mu(R)$ is obtained from solving the coupled equations

$$\left(\frac{\partial^2}{\partial R^2} + \frac{1}{4R^2} + 2\mu E - U_\mu(R)\right)F_\mu(R) + \sum_{\nu} W_{\mu\nu}(R)F_\nu(R) = 0 \tag{11}$$

where the coupling terms are

$$W_{\mu\nu} = 2\langle\Phi_\mu|\frac{\mathrm{d}}{\mathrm{d}R}|\Phi_\nu\rangle\frac{\mathrm{d}}{\mathrm{d}R} + \langle\Phi_\mu|\frac{\mathrm{d}^2}{\mathrm{d}R^2}|\Phi_\nu\rangle.$$

The coupling terms are small in general except in the local avoided crossing region. These terms are not included in the present article where we analyse the qualitative behaviour of a number of systems. In a more precise calculation and in scattering calculations for individual systems these terms should be included.

## 3. Finite element methods for solving the channel functions

In order to obtain accurate calculations for the bound and resonance states of an ABC system using the hyperspherical approach, it is essential to solve the adiabatic channel functions and the eigenvalues accurately. Previously the partial differential equations (10) were solved using some simple basis functions (Chen and Lin 1990). Because of the singularity of the Coulomb potential, the accuracy of the calculated eigenvalues is limited to two or three digits.

The two-dimensional partial differential equations (10) are solved by the finite element method (FEM) (Bathe and Wilson 1976, Bathe 1982, Shertzer and Levin 1991 and Botero and Shertzer 1992). In the FEM method, the domain of the two-variable function $F(x, y)$ is divided into rectangular elements. Within each element $\epsilon$, the function $F(x, y)$ is expanded in a local basis:

$$F(x, y) = \sum_{j=1}^{N} U_j^\epsilon e_j^\epsilon(x, y) \tag{12}$$

where $e_j^\epsilon(x, y) = g_j^\epsilon(x)h_j^\epsilon(y)$, with $g$ and $h$ each being a polynomial. The expansion coefficients $U_j^\epsilon$ are the values of $F(x, y)$, $\partial F/\partial x$, $\partial F/\partial y$, and $\partial^2 F/\partial x\partial y$ at the nodes of the element. In this work, we choose nine nodes for each element $\epsilon$—four at the corners, one each at the midpoint of each side and another at the centre of the rectangle. Each local basis function $g$ and $h$ is a fifth-order polynomial.

To determine the coefficients of the polynomials in the local basis function, consider the domain of the element $\epsilon$ to be a square of unit length. If $U_1$ is the value of $F$ at $(x, y) = (0, 0)$, and $F = (a_0 + a_1x + ... + a_5x^5)(b_0 + b_1y + .. + b_5y^5)$ is the expansion for the element $\epsilon$, the coefficients $a$ are determined by requiring that $F = 1$ at $(x, y) = (0, 0)$, and $F = 0$ at $(\frac{1}{2}, 0)$ and $(1, 0)$ and $\partial F/\partial x$=0 at these points. Similarly the $b$ can be determined by the same conditions at the three points along the $y$-axis. Applying this procedure to each node allows the determination of the 36 local basis functions within the element.

Substitution of the expansion (12) into the Schrödinger equation (10) allows the construction of a local matrix. After summing over all the elements and mapping local indices to global indices, a global matrix is obtained which can be diagonalized to obtain the eigenvalues. Since there are four unknowns at each node, the dimension of the matrix is roughly equal to the total number of nodes on the $(\phi, \theta)$ plane multiplied by four.

The partial differential equations (10) can be expressed in terms of either of the three sets of Jacobi coordinates. Typically we use the $\alpha$-set coordinates for the small $R$ region, and either $\beta$ or $\gamma$ sets for the large $R$ region. The $\phi$ range $(0 \leqslant \phi \leqslant \pi/2)$ is typically divided into 25 segments, and the range of $\theta(0 \leqslant \theta \leqslant \pi)$ is typically divided into 10 segments, thus there are about 250 elements and the size of the matrix is a sparse matrix of order 4032. We can achieve typically five digits accuracy in the potential curves in the small $R$ region and four digits in the larger $R$ region with the present method. In general, the accuracy is better for systems where one particle is much heavier than the other two. This accuracy is related to the singular structure of the potential surface in the mass-weighted hyperspherical coordinates.

## 4. Results and discussion

For the three-body systems, ABC, we choose $m_C = 1$, $m_A = 26.585$ and study the evolution of the systems as the mass $m_B$ varies from $m_C$ to $m_A$. Thus if $m_A = m_B$, the system corresponds to a tt$\mu$ ion where the mass of the muon is set to unity. Similarly, $m_B = 17.75(8.88)$, corresponds to a dt$\mu$ (pt$\mu$) system. If $m_B$=1, it is a t$\mu^+\mu^-$ system. We will also consider a xt$\mu$ system, with the mass of x being $m_x = 3$, as an intermediate case.

### *4.1. Potential curves*

We first study the two lowest potential curves for the four systems dt$\mu$, pt$\mu$, xt$\mu$ and t$\mu^+\mu^-$ for the case of total angular momentum $L = 0$ and even parity. The results are shown in figure 3. In the asymptotic region, the lowest curve corresponds to the limit of $B^+(t\mu^-)_{1s}$ where $(t\mu^-)_{1s}$ is the two-body 'hydrogenic 1s' state between the two particles t and $\mu^-$, with the energy given by 0.9637 Ryd. Similarly, the second lowest curve corresponds to the limit of $t^+(B\mu^-)$ , with the energy given by $m_{B\mu} = m_B/(1 + m_B)$ Rydbergs. We actually renormalize the energy scale in figure 3 so that the lowest curve for each system approaches the asymptotic energy of $-1.0$ Ryd.

From these four systems, it is clear that the lowest potential curve is more attractive and the second lowest potential curve is more repulsive when $m_B \simeq m_A$. This result is also related to the fact that the two curves are quite close to each other in the asymptotic region when $m_B \simeq m_A$. As $m_B$ becomes smaller, the two curves in the asymptotic region becomes more separated, and each curve shows only a shallow potential well.

The locations of the potential minimum for the curves shown in figure 2 differ quite significantly. This difference is mostly due to the mass scaling of the hyperradius. Since

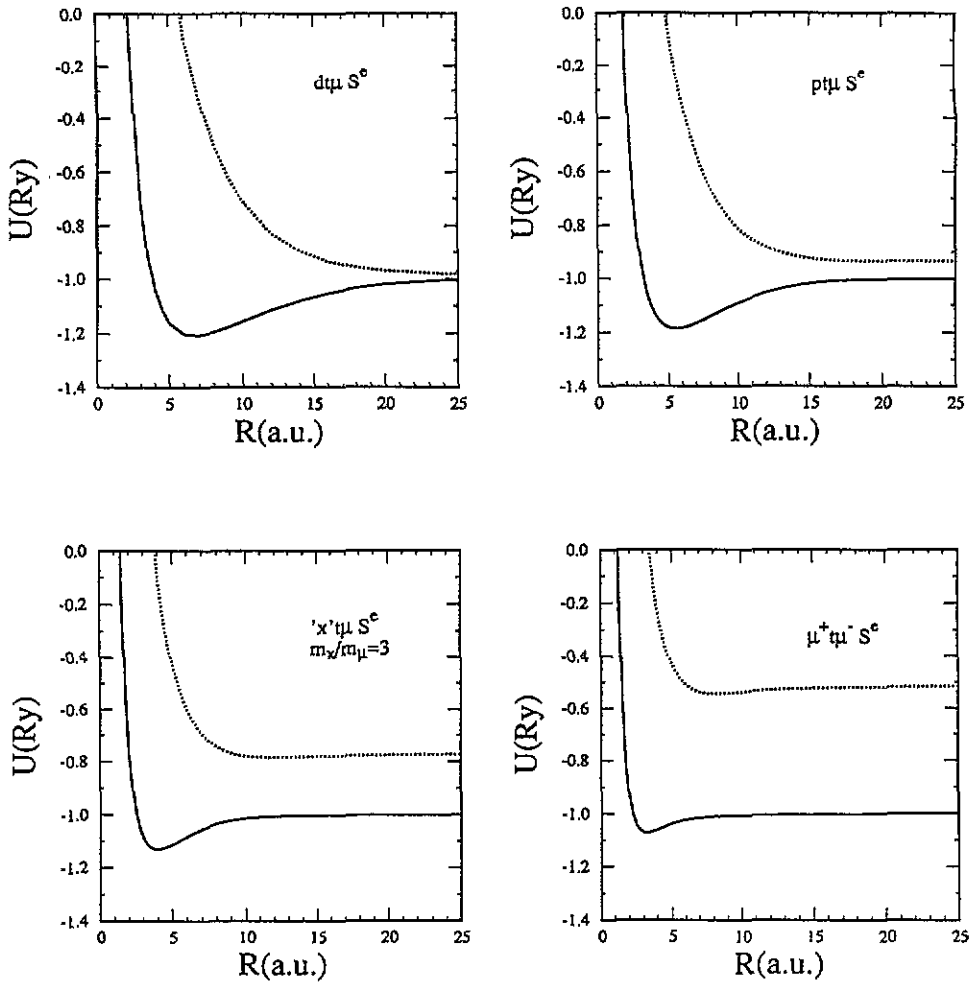


**Figure 3.** The adiabatic potential curves for the four systems indicated. The total angular momentum of the system is zero and the energies calculated have been renormalized so that the lowest curve approaches −1.0 Ryd in the asymptotic limit.

the lowest curve corresponds to the B + (AC) dissociation limit, it is convenient to use the $\gamma$-set coordinates to describe this channel. (All the variables in this paragraph refer to $\gamma$-set coordinates hereafter.) The potential minimum occurs when $\rho_1 \simeq \rho_2$ so that $R^2 = (\mu_1\rho_1^2 + \mu_2\rho_2^2)/\mu \simeq (\mu_1 + \mu_2)\rho_1^2/\mu$. Since the length scale of $\rho_1$ is inversely proportional to the reduced mass $\mu_1$, the hyperradius where the potential curve reaches the minimum is proportional to $\sqrt{(\mu_1 + \mu_2)}/\mu_1$. If we use the $R_{\min} = 6.75$ from the calculated value for dt$\mu$, then the corresponding $R_{\min}$ for the pt$\mu$, xt$\mu$ and t$\mu^+\mu^-$ systems are 5.45, 3.77 and 2.73, respectively, which are in good agreement with the values actually calculated shown in figure 3.

For $L = 0$, the dt$\mu$ system is known to support two bound states. This means that the lowest potential curve for dt$\mu$ in figure 3 can support two bound states. For the pt$\mu$ system, the curve is supposed to support one bound state. A simple procedure to estimate the number of bound states is to calculate the classical action

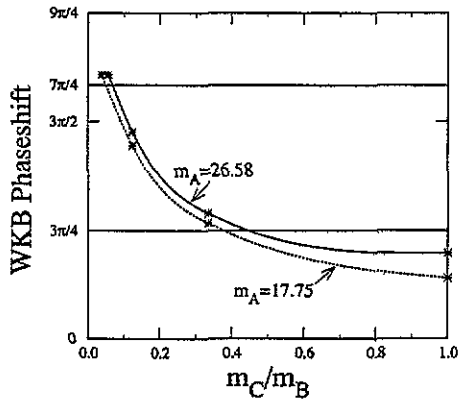


**Figure 4.** The phaseshift as defined in equation (13) for $E = -1.0$, i.e. at the threshold. The symbols * are phaseshifts obtained from calculated adiabatic potential curves and the lines are obtained by interpolation. The two horizontal lines correspond to phaseshifts of $\frac{3}{4}\pi$ and $\frac{7}{4}\pi$. If the phaseshift is below the first horizontal line, then no stable bound state exists. If the phaseshift is between the two horizontal lines, then there is one bound state. The mass of particle C is set at 1.0 and the mass of particle A is shown.

$$I = 2\int_{R_1}^{R_2} [E - U_1(R)]\mathrm{d}R \tag{13}$$

at the threshold energy ($E = -1.0$), where $R_1$ is the inner classical turning point and $R_2$ is the outer turning point which was set at infinity. For the existence of $(n+1)$ bound states, the classical action (or the zero-energy phaseshift) has to be greater than $(n+\frac{3}{4})\pi$. In figure 4 we plot $I$ against $1/m_B$ for the above four systems where $m_A = 26.58$ and another four systems with the same $m_B$ and $m_C$, but with $m_A = 17.75$. From the phaseshifts of the four calculated systems an interpolated phaseshift curve is obtained for each $m_A$. Two horizontal lines corresponding to phaseshift of $\frac{3}{4}\pi$ and $\frac{7}{4}\pi$ are also indicated. For a given $m_B$, if the phase shift is below $\frac{3}{4}\pi$, there will be no bound state. If the phaseshift is between $\frac{3}{4}\pi$ and $\frac{7}{4}\pi$, there will be one bound state. According to our calculated phase shifts, we conclude that there is no bound state for the $t\mu^+\mu^-$ system, one bound state for the $xt\mu$ and $pt\mu$ systems, and two bound states for the $dt\mu$ system. This conclusion is consistent with the results obtained from variational calculations for the $dt\mu$ and $pt\mu$ systems (Frolov 1987). The binding energies for the other two systems have not been calculated. From the curve for $m_A = 17.75$, we can conclude also that there is one bound state for $pd\mu$ and one bound state for $xd\mu$, and no bound state for $d\mu^+\mu^-$. The result of one bound state only for $pd\mu$ is also consistent with the variational calculations. According to this estimate, the mass of particle B has to be greater than 2.22 for a bound state to exist if $m_A = 26.58$ and $m_C = 1.0$. The critical mass for particle B is 2.63 if $m_A = 17.75$ and $m_C = 1.0$. (The actual masses of the protons, deuterons, tritons and muons are 1836.1515, 3670.481, 5496.918 and 206.769 in atomic units.)

### *4.2. Density plots*

We have discussed that the two potential curves in the asymptotic limit correspond to the dissociation of the three-body system into B+(AC) for the lowest curve, and into A+(BC) for the second curve. In this limit, the wave function, or density, should concentrate at the two potential valleys around $\phi_1$ and $\phi_2$, respectively. However, it is not clear at what

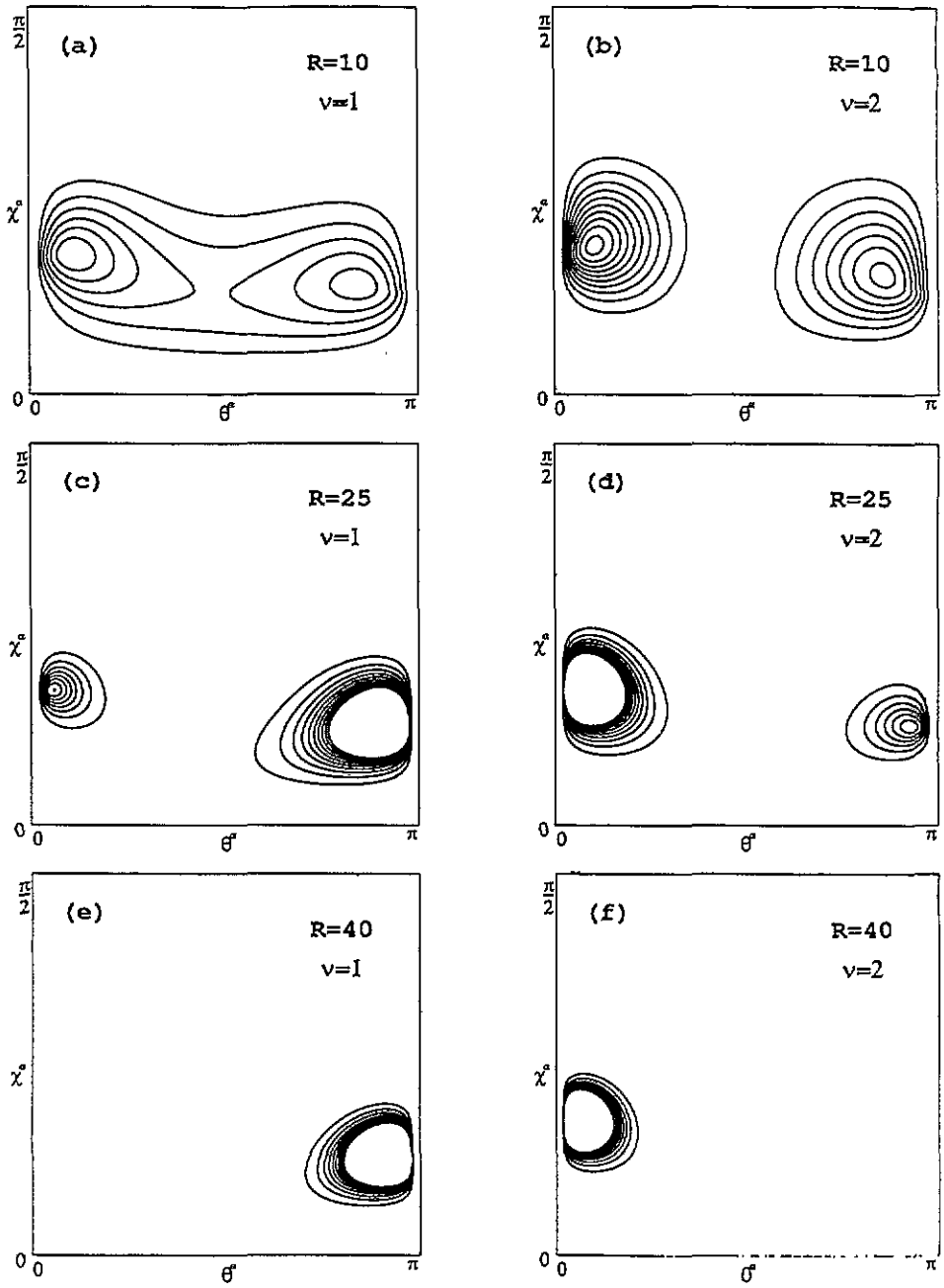


**Figure 5.** The density distribution of the two lowest channels for the dt$\mu$ system ($L = 0$) at three different values of $R$. At $R = 10$ where the lowest potential is near its minimum, the density distribution covers most of the $(\chi^\alpha, \theta^\alpha)$ plane. The $\nu = 1$ and $\nu = 2$ channels show resemblance to the bonding and antibonding states in that $\theta = \pi/2$ is nearly an antinodal line for the $\nu = 1$ channel and a nodal line for the $\nu = 2$ channel. Note that at $R = 25$ where the potential curves are approaching the asymptotic limit, there is still a significant probability of finding the particle C near both centres. Only at $R = 40$ is particle C bound to particle A for $\nu = 1$ and to particle B for $\nu = 2$.

distance this separation occurs, since at smaller values of $R$ the density is expected to occupy most of the $(\phi, \theta)$ plane. In figure 5 we show the density plots of the dt$\mu$ system at R=10, 25 and 40. It is clear that at $R = 10$, the density distribution for the lowest channel occupies most of the $(\chi, \theta)$ plane. In fact, the lowest curve displays bonding nature in that particle C has a large probability in the region between the two potential valleys, while for the second lowest channel, there is a nodal line in this region, similar to an antibonding state. Notice that these bonding and antibonding characters become exact if particles A and B are identical. At $R = 25$ where the potential curves are quite close to the asymptotic region already, we notice that there is still a large probability for finding $\mu$ near d in the lowest channel, and for finding $\mu$ near t in the second lowest channel. Only at $R = 40$ do we begin to see that the muon is attached exclusively to one centre or another.

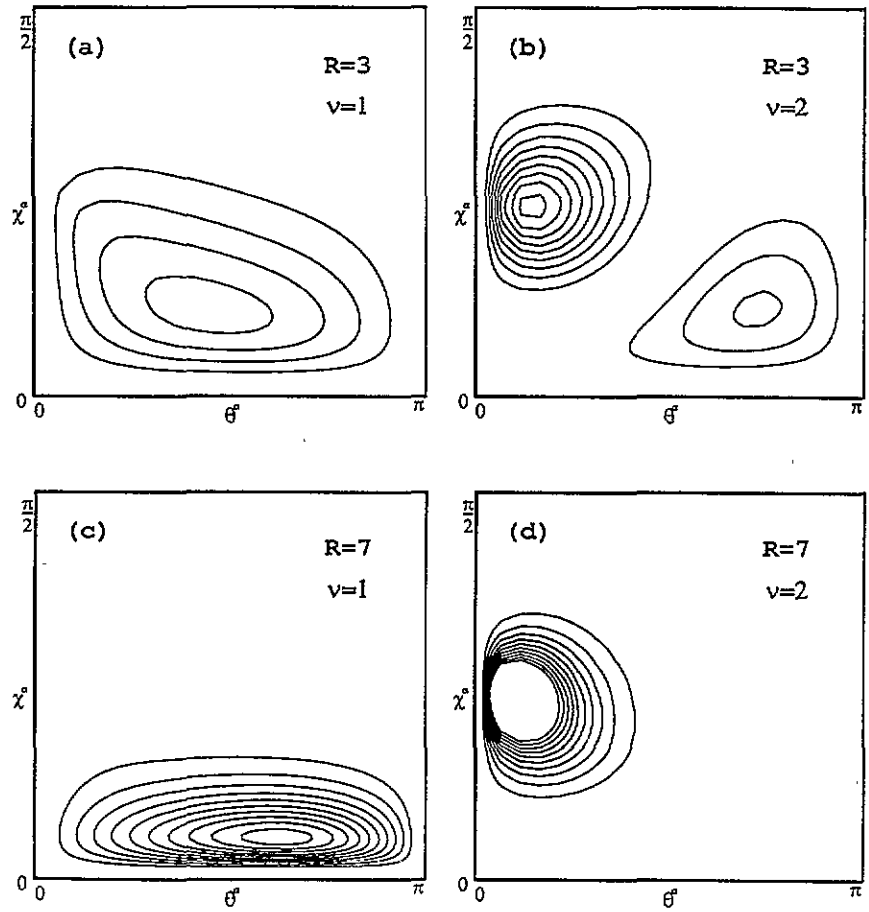


**Figure 6.** Similar density distributions for the $t\mu^+\mu^-$ system at two different values of $R$. At $R = 3$, there is indication of antinodal and nodal lines for $\nu = 1$ and $\nu = 2$, respectively, except that the line is curved in the $(\chi^a, \theta^a)$ plane. The breakup of this system into one particle and another pair occurs at small $R$. The lower frame shows that the breakup into $\mu^+ + (t, \mu^-)$ for $\nu = 1$ and $t + (\mu^+, \mu^-)$ for $\nu = 2$ occurs at $R = 7$.

We next examine the situation for $t\mu^+\mu^-$. As can be seen from figure 2, the singularity of one of the two potential valleys is very close to the $\chi = 0°$ axis, while the other is at

$\chi = 44°$. In figure 6(*a*) and (*b*), the density plots for the two channels at $R = 3$ are shown. The lowest channel does show that the density lies between the two potential valleys (see figure 2(*d*)), while for the upper channel, a distinct nodal line is seen lying perpendicular to the curve which is the locus of the local potential minimum. Compared to figure 5(*a*) and (*b*), the bonding and anti-bonding characters are much less evident in the present case. In fact, at $R = 7$, the separation of the ground channel into $\mu^+ + (t\mu^-)$ and the second channel into $t + (\mu^+\mu^-)$ is already quite evident. The large energy separation between the ground state of $(t\mu^-)$ and of $(\mu^+\mu^-)$ in comparison with the exchange energy of the negative muon between the two positively charged centres is responsible for the lack of stability of this three-body system.

### *4.3. Non-adiabatic coupling terms*

The two adiabatic potential curves shown in figure 3 display pronounced avoided crossings similar to those considered by Demkov for near-resonance charge exchange processes in ion–atom collisions. The non-adiabatic coupling term $\langle\Phi_1|d/dR|\Phi_2\rangle$ shows a sharp avoided crossing at 24, 15, 8 and 4.5, respectively, for the four systems shown. The location of this avoided crossing occurs when the exchange energy of the negative charged particle with respect to the two positive charges is about equal to the energy separation of the two channels at large $R$. We mention that the 'muon transfer' probability is determined by this non-adiabatic coupling.

## 5. Summary and conclusions

In this paper we discussed the application of mass-weighted hyperspherical coordinates to Coulombic three-body systems where all three particles are different. We applied adiabatic approximation to calculate the potential curves and examined the corresponding channel wavefunctions for the lowest two channels. By fixing the masses of two of the particles we studied how the adiabatic potential curves, the density distribution of the channel functions and the non-adiabatic coupling terms of the three-body systems evolve as the mass of the third particle is varied. We also demonstrated the use of higher order finite element method for calculating eigenvalue problems in two dimensions. The existence of bound states for Coulombic three-body systems was examined from the calculated potential curves.

As stated in the introduction, our main goal is to develop a computational procedure for carrying out calculations of inelastic and rearrangement collision cross sections involving three charged particles using hyperspherical coordinates. Such calculations have been carried out for the two-electron atomic systems where no rearrangement channels exist and where the mass of the nucleus is taken to have infinite mass (Tang *et al* 1992, Zhou *et al* 1993). The extension of the hyperspherical close-coupling method to three particles of any masses involves additional complications. In this paper we illustrated that the finite element method can be used to obtain accurate adiabatic potential curves. We are currently extending the method to states of non-zero angular momentum and treating the matching of the hyperspherical solutions to the single particle states in the asymptotic region to extract the scattering matrix.

## Acknowledgments

This work is supported in part by the US Department of Energy, Office of Energy Research, Division of Chemical Sciences (YZ and CDL) and in part by the National Science Foundation (JS).

## References

Archer B J, Parker G A and Pack R T 1990 *Phys. Rev.* A **41** 1303
Avery J 1989 *Hyperspherical Harmonics, Application in Quantum Theory* (Dordrecht: Kluwer )
Bathe K 1982 *Finite Element Procedures in Engineering Analysis* (Englewood Cliffs, NJ: Prentice-Hall)
Bathe K and Wilson E 1976 *Numerical Methods of Finite Element Analysis* (Englewood Cliffs, NJ: Prentice-Hall)
Berry R S and Krause J L 1988 *Adv. Chem. Phys.* **70** 35
Bishop D M and Frolov A M 1992 *J. Phys. B: At. Mol. Opt. Phys.* **25** 3049
Botero J and Greene C H 1985 *Phys. Rev.* A **32** 1249
Botero J and Shertzer J 1992 *Phys. Rev.* A **46** R1155
Chen Z and Lin C D 1990 *Phys. Rev.* A **42** 18
Frolov A M and Thakkar A J 1992 *Phys. Rev.* A **46** 4418
Frolov A M 1987 *Zh. Eksp. Teor. Fiz.* **92** 1959 (Engl. transl. *Sov. Phys.–JETP* **65** 1100)
Fukuda H, Ishihara T and Hara S 1990 *Phys. Rev.* A **41** 145
Gur'yanov A V and Rebane T K 1991 *Opt. Spectrosc.* **70** 419
Herrick D R, Kellman and Poliak R D 1980 *Phys. Rev.* A **22** 1517
Hill R N 1977 *J. Math. Phys.* **18** 2316
Hara S, Fukuda H, Ishihara T and Matveenko A V 1988 *Phys. Lett.* **130** 22
Hara S and Ishihara 1989 *Phys. Rev.* A **40** 4232
Launay J M and Le Dourneuf M 1989 *Chem. Phys. Lett.* **163** 178
—— 1990 *Chem. Phys. Lett.* **169** 473
Lin C D 1984 *Phys. Rev.* A **29** 1019
—— 1986 *Adv. At. Mol. Phys.* **22** 77
Lin C D and Liu X H 1988 *Phys. Rev.* A **37** 2749
Liu X H, Chen Z and Lin C D 1991 *Phys. Rev.* A **44** 5468
Martin A, Richard J M and Wu T T 1992 *Phys. Rev.* A **46** 3697
Pack R T and Parker G A 1989 *J. Chem. Phys.* **90** 3511
Poshusta R D 1985 *J. Phys. B: At. Mol. Phys.* **18** 1887
Rost J M and Briggs J 1991 *J. Phys. B: At. Mol. Opt. Phys.* **24** 4293
Shertzer J and Levin F S 1991 *Phys. Rev.* A **43** 2531
Tang J Z, Watanabe S, Matsuzawa M and Lin C D 1992 *Phys. Rev. Lett.* **69** 1633
Zhou B, Lin C D,Tang J Z, Watanabe S and Matsuzawa M 1993 to be published